Theor Chem Acc (2007) 117:579–586
DOI 10.1007/s00214-006-0244-8

REGULAR ARTICLE

Radical–molecule reaction $CH_2Cl + NO_2$: a mechanistic study

Jia-xu Zhang · Ze-sheng Li · Jing-yao Liu · Chia-chung Sun

Received: 30 March 2006 / Accepted: 22 November 2006 / Published online: 10 January 2007

Abstract The radical–molecule reaction mechanism of CH_2Cl with NO_2 has been explored theoretically at the B3LYP/6–311*G*(d,p) and MC–QCISD (single-point) levels of theory. Our results indicate that the title reaction proceeds mostly through singlet pathways, less go through triplet pathways. The initial association between CH_2Cl and NO_2 is found to be the carbon-to-nitrogen attack forming the adduct **a** H_2ClCNO_2 with no barrier, followed by isomerization to $\mathbf{b_1}$ $H_2ClCONO$-*trans* which can easily convert to $\mathbf{b_2}$ $H_2ClCONO$-*cis*. Subsequently, the most feasible pathway is the C–Cl and O–N bonds cleavage along with the N–Cl bond formation of **b** ($\mathbf{b_1}, \mathbf{b_2}$) leading to product $\mathbf{P_1}$ $CH_2O + ClNO$, which can further dissociate to give $\mathbf{P_5}$ $CH_2O + Cl + NO$. The second competitive pathway is the 1,3-H-shift associated with O–N bond rupture of $\mathbf{b_1}$ to form $\mathbf{P_2}$ $CHClO + HNO$. Because the intermediates and transition states involved in the above two favorable channels all lie below the reactants, the $CH_2Cl + NO_2$ reaction is expected to be rapid, as is confirmed by experiment. The present results can lead us to understand deeply the mechanism of the title reaction and may be helpful for further experimental investigation of the reaction.

Keywords Theoretical calculations · Reaction mechanism · Potential energy surface (PES) · Chloromethyl (CH_2Cl) · Nitric dioxide (NO_2)

J. Zhang · Z. Li (✉) · J. Liu · C. Sun
Institute of Theoretical Chemistry, State Key Laboratory of Theoretical and Computational Chemistry, Jilin University, Changchun 130023, People's Republic of China
e-mail: Zeshengli@mail.jlu.edu.cn

1 Introduction

Nitrogen oxides, known to be the major atmospheric pollutants released by combustion process, have attracted extensive attentions both experimentally and theoretically. In order to minimize the harmful effects before their release in the atmosphere, one effective way is to reduce them chemically by their reactions with other species [1–7]. Chlorinated hydrocarbon species such as CH_2Cl, $CHCl_2$, and CCl_3 radicals are important intermediates in combustion processes, especially during incineration of hazardous waste [8]. In addition, the chlorinated hydrocarbons increase soot formation in fuel-rich oxidation [9]. These species can be formed in unimolecular decomposition reactions of stable chlorinated hydrocarbon molecules under combustion conditions. Bond-breaking reactions for the stable chlorinated compounds occur uniformly at lower temperatures than for the hydrocarbons of similar size. Radical–radical cross-combination reactions constitute an integral part of the overall mechanisms of oxidation and pyrolysis of hydrocarbons [10,11]. Reactions of chlorinated methyl radicals with other radicals are important in the combustion of chlorinated hydrocarbons. Kinetic stability of the methyl radical increases in the combustion environment as one or more hydrogen atoms in the radical are substituted by chlorine atoms, because peroxy adducts formed via radical addition to O_2 increasingly favor decomposition back to the radical and O_2 as chlorine substitution increases [12]. This is due to the weaker C–O bond in the chlorinated peroxy adducts than in their hydrocarbon counterparts, thus increasing the importance of reactions of chlorinated methyl radicals with species other than molecular oxygen. Reactions with NO_2 can be expected to be important during the

oxidation of chlorinated compounds at low temperatures, because traces of nitrogen oxides are also often present [13]. Hence, reliable information on the kinetics of these chlorinated methyl radical reactions is of importance for the modeling of NO_x-involved reaction processes.

The direct kinetic studies of the substituted methyl radical reactions with NO_2 is few. Very recently, Timonen et al. [14] reported for the first time the direct kinetic studies of $CH_2Cl + NO_2$ reaction over temperature ranges (220–360 K) using a tubular flow reactor coupled with a photoionization mass spectrometer and derived the rate constant expression as $(2.16 \pm 0.08) \times 10^{-11}$ $(T/300\,K)^{-1.12\pm0.24}$ cm^3 $molecule^{-1}$ s^{-1}, which indicate that the reaction of CH_2Cl with NO_2 is very rapid and may play an important role in the fate of nitrogen dioxide pollutants. The observed major product was CH_2O. In addition, a weak signal for the NO formation has also been detected for this reaction [14]. However, the available information on product channels, product distributions, and reaction mechanism were not further provided though this information may be important in the NO_2-involved sequential chain processes. To our best knowledge, no report is found about the theoretical study on the title reaction. In view of the potential importance and the rather limited information, we carry out a detailed theoretical study on the potential energy surface (PES) of the $CH_2Cl + NO_2$ reaction to (1) provide the elaborated isomerization and dissociation channels on the H_2ClCNO_2 PES; (2) investigate the products of the title reaction to assist in further experimental identification; (3) give a deep insight into the mechanism of the reaction of chloromethyl with nitrogen dioxide.

2 Computational methods

All calculations are carried out using the GAUSSIAN03 program packages [15]. The geometries of all the reactants, products, intermediates, and transition states are optimized using the hybrid density functional B3LYP method (Becke's three parameter hybrid functional with the nonlocal correlation functional of Lee–Yang–Par) with 6–311G(d,p) basis set. The stationary nature of structures is confirmed by harmonic vibrational frequency calculations; i.e., equilibrium species possess all real frequencies, whereas transition states possess one and only one imaginary frequency. The zero-point energy (ZPE) corrections are obtained at the same level of theory. In order to obtain more reliable energetic data, higher level single-point energy calculations are performed at the multi-coefficient correlation method based on quadratic configuration interaction with single and double excitations (MC–QCISD) [16] by using the B3LYP/6–311G(d,p) optimized geometries. To confirm that the transition states connect designated isomers or products, intrinsic reaction coordinate (IRC) calculation is carried out at the B3LYP/6–311G(d,p) level. Moreover, unless otherwise specified, the MC–QCISD single-point energies with ZPE corrections are used in the following discussions. Meanwhile, for the purpose of comparison, we employed the higher level G2(B3LYP/MP2/CC) [17] (a modification of the Gaussian-2 approach using density functional theory) to calculate the single-point energy based on the B3LYP/6–311G(d,p) geometries. The total G2(B3LYP/MP2/CC) energy with ZPE correction is calculated as follows [17]:

$$\begin{aligned} &E[\text{G2(B3LYP/MP2/CC)}] \\ &\quad = E[\text{CCSD(T)/6–311}G\text{(d,p)}] + E[\text{MP2/6–311} \\ &\qquad +G\text{(3df,2p)}] - E[\text{MP2/6–311}G\text{(d,p)}] \\ &\qquad +\text{HLC} + \text{ZPE[B3LYP/6–311}G\text{(d,p)}] \times 0.98, \end{aligned}$$

where $\text{HLC} = -0.00451n_\beta - 0.00019n_\alpha$, and n_α and n_β denote the numbers of α and β valence electrons, respectively.

3 Results and discussion

The optimized structures of important stationary points as well as the corresponding experimental data [18,19] are depicted in Fig. 1. Note that the calculated geometries are in good agreement with experimental results with the largest deviation less than 7 at the B3LYP/6–311G(d,p) level. Table 1 displays the relative energies including ZPE corrections of the important stationary points. For our discussion easier, the energy of reactants **R** is set to be zero for reference. For the title reaction, both reactant molecules are doublet and the spin contamination is not severe; i.e., the $\langle S^2 \rangle$ values of CH_2Cl and NO_2 are less than 0.76, very close to the expected value of the pure double state 0.75. To clarify the reaction mechanism, the relevant pathways of the singlet PES for $CH_2Cl + NO_2$ reaction are depicted in Fig. 2.

3.1 Initial association

Both singlet and triplet CH_2ClNO_2 PES may be obtained for the radical–molecule reaction of CH_2Cl $(C_{2v}, {}^2B_1) + NO_2(C_{2v}, {}^2A_1)$. On the singlet PES, the carbon-to-nitrogen approach is rather attractive to form structure **a** $H_2ClCNO_2(C_s, {}^1A')$ without any encounter barrier. The association is expected to be fast and to play a significant role in the reaction kinetics. For

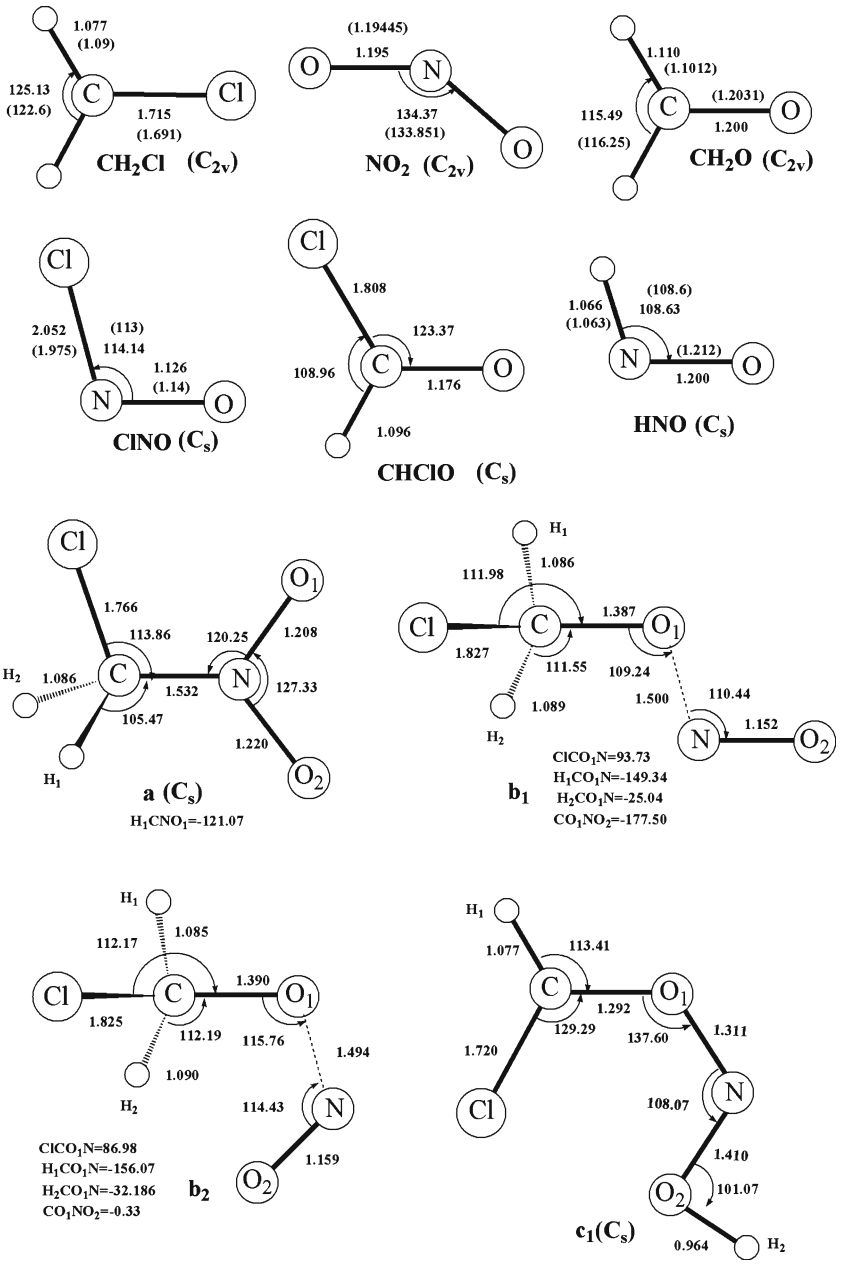

Fig. 1 The B3LYP/6–311*G*(d,p) optimized geometries of reactants, some important products, isomers, and transition states for $CH_2Cl + NO_2$ reaction. The values in *italics* are for the triplet species. Bond distances are in angstroms and angles are in degrees. The values in *parentheses* are the experimental values ([18] for NO_2, CH_2O, [19] for CH_2Cl, ClNO, HNO). In the transition states the direction of the imaginary frequency is indicated by "⇌"

the carbon-to-oxygen approach, we cannot obtain any transition state, linking the reactants **R** to the isomers **b1** H2ClCONO-*trans* and **b2** H2ClCONO-*cis* despite a lot of attempts. Yet, we except that considerable barrier is needed to activate the short N = O double bond (1.195 Å) in NO_2 to form the long N–O weak bond in **b** (1.500 Å in **b1**, 1.494 Å in **b2**). Instead, **b1** H2ClCONO-*trans* can be barrierlessly formed from **R** via the intermediate **a**, as shown in Fig. 2. On the other hand, the carbon-to-nitrogen approach on the triplet PES can lead to the triplet isomer ^{3}**a** H_2ClCNO_2 (13.4 kcal/mol) via the transition state ^{3}**TSRa** with the much higher barrier of 35.3 kcal/mol and there is a substantial barrier of 21.0 kcal/mol for the carbon-to-oxygen attack to form isomer ^{3}**b1** H2ClONO-*trans* (0.4 kcal/mol). In view of the much higher entrance barriers, the triplet pathways may contribute less to the $CH_2Cl + NO_2$ reaction compared with the singlet pathways, and thus will not be further discussed. As a result, the carbon -to-nitrogen approach forming isomer **a** H_2ClCNO_2 on the singlet PES is just the initial adduct step of all the calculated pathways in our work. In the following, we mainly

Fig. 1 continued

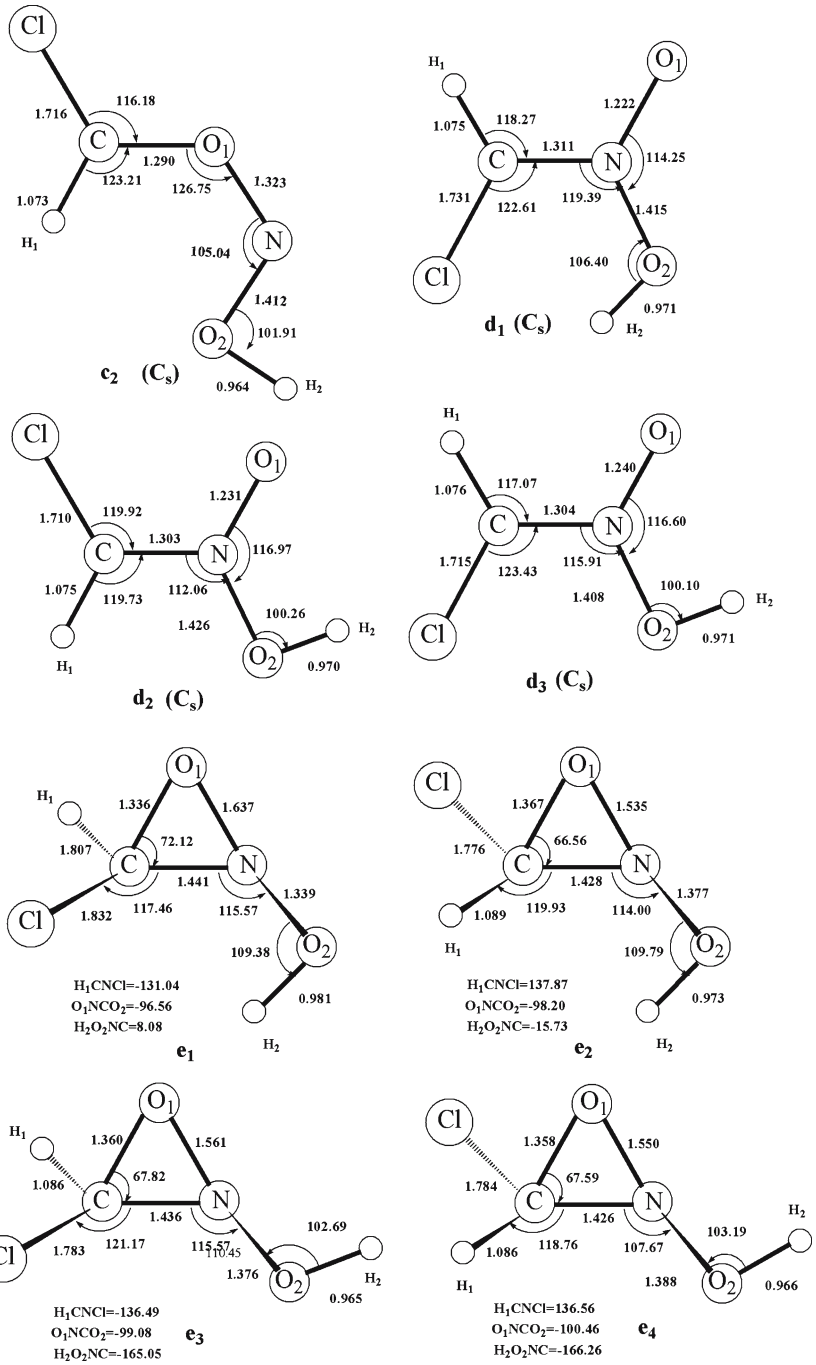

discuss the formation pathways of various products proceeding via isomer **a**.

3.2 Isomerization and dissociation pathways

As shown in Fig. 2, the chainlike isomer **a** H_2ClCNO_2 may prefer undergoing the C–O1 bond formation along with the C–N bond rupture via **Tsab$_1$** (C_s, $^1A'$) leading to another chainlike intermediate **b$_1$** $H_2ClCONO$-*trans*, which can easily convert to **b$_2$** $H_2ClCONO$-*cis*. A barrier of 48.2 kcal/mol is needed to overcome for the conversion from **a** $\rightarrow$ **b$_1$**. As shown in Fig. 1, the transition state **TSab$_1$** has a loose CNO1 three-membered ring structure, in which the distance of C–O1 is surprisingly long as 2.381 Å, while the C–N bond that will be broken is 1.535 Å . Subsequently, isomer **b** (**b$_1$**, **b$_2$**) can dissociate to give product **P$_1$** $CH_2O(C_{2v}, ^2A_1)+ClNO(C_s, ^1A')$ via C–Cl and O1–N bonds cleavage accompanied by the

Fig. 1 continued

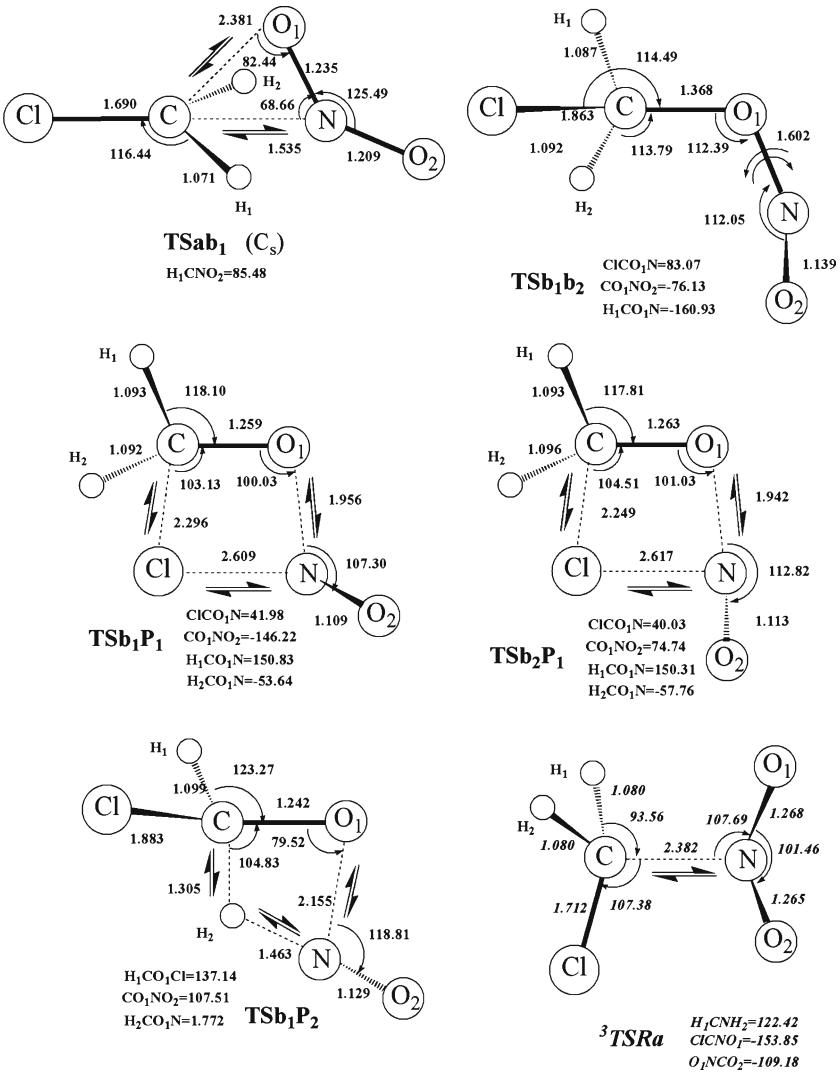

N–Cl bond formation through transition states $\mathbf{TSb_1P_1}$ and $\mathbf{TSb_2P_1}$. The dissociation barriers are 23.9 and 24.5 kcal/mol for $\mathbf{b_1} \rightarrow \mathbf{P_1}$ and $\mathbf{b_2} \rightarrow \mathbf{P_1}$, respectively. Both $\mathbf{TSb_1P_1}$ and $\mathbf{TSb_2P_1}$ present a loose ClCO1N four-membered ring structure, which is nonplanar. The forming Cl–N bond lengths are 2.609 and 2.617 Å, respectively, while the breaking C–Cl and O1–N distances are 2.296 and 1.956 Å (in $\mathbf{TSb_1P_1}$), 2.249 and 1.942 Å (in $\mathbf{TSb_2P_1}$). Alternatively, the isomer $\mathbf{b_1}$ can take a 1,3-H-shift and O1–N bond rupture leading to $\mathbf{P_2}$ $CHClO(C_s, {}^1A')$+$HNO(C_s, {}^1A')$ via $\mathbf{TSb_1P_2}$ with the barrier height 35.9 kcal/mol. The loose H2CO1N four-membered ring, which is slightly nonplanar is found in $\mathbf{TSb_1P_2}$. The migrating hydrogen is 1.321 Å away from the origin (C atom) and 1.475 Å away from the migrating terminus (N atom), and the O1–N bond that will be broken is surprisingly long as 2.081 Å . In addition, the primary product $\mathbf{P_1}$ can further dissociate to give $\mathbf{P_5}$ $CH_2O(C_{2v}, {}^2A_1) + Cl + NO(C_{\infty v}, {}^2\prod)$ via the direct N–Cl single bond rupture. These processes can be described as

$$\mathbf{Path1}: \mathbf{R} \rightarrow \mathbf{a} \rightarrow \mathbf{b}(\mathbf{b_1}, \mathbf{b_2}) \rightarrow \mathbf{P_1} CH_2O + ClNO \rightarrow \mathbf{P_5}\ CH_2O + Cl + NO$$

$$\mathbf{Path2}: \mathbf{R} \rightarrow \mathbf{a} \rightarrow \mathbf{b_1} \rightarrow \mathbf{P_2} CHClO + HNO.$$

As shown in Fig. 2, in terms of adiabatic potential energy, all the transition states and isomers in **Path 1** and **Path 2** lie below the reactants **R**. As a result, **Paths 1** and **2** are favorable at normal temperature and the title reaction will occur barrierlessly with respect to the reactants.

Now, we turn our attention to the other isomerization and dissociation channels of the isomers **a** and $\mathbf{b_2}$. First, a 1,3 H-shift from C-atom to O_2-atom associated with a concert twist of **a** can form $\mathbf{d_1}$ or $\mathbf{d_2}$. Isomers $\mathbf{d_1}$, $\mathbf{d_2}$, and $\mathbf{d_3}$ are *cis–trans* species for the $HClCN(O)OH$ $(C_s, {}^1A')$ structure in terms of C-bound chlorine or O-bound

Table 1 The relative energies (kcal/mol) [with inclusion of the B3LYP/6–311*G*(d,p) zero-point energy (ZPE) corrections] of reactants, some important products, isomers, and transition states at the MC–QCISD//B3LYP/6–311*G*(d,p) and G2(B3LYP/MP2/CC)//B3LYP/6–311*G*(d,p) levels

Species	MC–QCISD	G2 (B3LYP/MP2/CC)
R CH_2Cl $(C_{2v},{}^2B_1) + NO_2(C_{2v},{}^2A_1)$	0.0	0.0
P₁ CH_2O $(C_{2v},{}^2A_1) + ClNO(C_s,{}^1A')$	−50.3	−52.0
P₂ CHClO $(C_s,{}^1A') + HNO(C_s,{}^1A')$	−57.5	−57.9
P₅ $CH_2O(C_{2v},{}^2A_1)$ $+Cl + NO(C_{\infty v},{}^2\prod)$	−14.8	−14.4
a$(C_s,{}^1A')$	−53.1	−55.6
b₁	−58.0	−59.9
b₂	−56.7	−59.0
TSab₁$(C_s,{}^1A')$	−4.7	−3.1
TSb₁b₂	−47.5	−49.6
TSb₁P₁	−34.1	−36.1
TSb₂P₁	−32.2	−34.7
TSb₁P₂	−22.1	−25.8

hydrogen. Isomer $\mathbf{d_1}$ can readily convert to $\mathbf{d_3}$ via N–O_2 single bond rotation transition state $\mathbf{TSd_1d_3}$ with small barrier of 0.7 kcal/mol, while the conversion of $\mathbf{d_1}\rightarrow\mathbf{d_2}$ is a concerted process of C = N double bond and N–O_2 single bond simultaneous rotations via the transition state $\mathbf{TSd_1d_2}$ with the high barrier of 48.4 kcal/mol. Then, the ring-closure of $\mathbf{d_2}$ or $\mathbf{d_3}$ may lead to the three-membered ring isomer **e** HClC(O)NOH. Moreover, $\mathbf{d_2}$ can dissociate directly to give product $\mathbf{P_4}$ ClCNO $(C_s,{}^1A')+$ $H_2O(C_{2v},{}^2A_1)$ via side-H_2O cleavage. However, the conversion transition states $\mathbf{TSad_1}, \mathbf{TSad_2}, \mathbf{TSd_1d_2}$, $\mathbf{TSd_2e_2}, \mathbf{TSd_2e_4}, \mathbf{TSd_3e_1}, \mathbf{TSd_3e_3}$, and $\mathbf{TSd_2P_4}$ involved in these processes lie 11.0, 5.7, 10.7, 14.7, 15.2, 9.2, 9.7, and 10.6 kcal/mol higher than the reactants **R**, respectively. Clearly, the formation of **d** $(\mathbf{d_1}, \mathbf{d_2}, \mathbf{d_3})$, **e**$(\mathbf{e_1}, \mathbf{e_2}, \mathbf{e_3}, \mathbf{e_4})$, and $\mathbf{P_4}$ are less competitive than Paths 1 and 2 at room temperature. Furthermore, isomer $\mathbf{b_2}$ can take a concerted H-shift to form isomer **c**$(\mathbf{c_1}, \mathbf{c_2})$ HClCONOH $(C_s,{}^1A')$, which can dissociate to product $\mathbf{P_3}$CHClO $(C_s,{}^1A')$ + HON$(C_s,{}^1A')$. Because $\mathbf{TSb_2c_1}, \mathbf{TSb_2c_2}$, $\mathbf{TSc_1P_3}$ are 3.6, 5.8, and 3.2 kcal/mol higher than **R**, respectively, these pathways are also kinetically less feasible at normal temperature and have negligible contributions to the $CH_2Cl + NO_2$ reaction compared with the favorable pathways **Paths 1** and **2**.

3.3 Reaction mechanism and experimental implications

In the previous sections, we have obtained two important reaction channels (**Paths 1–2**) that are both thermodynamically and kinetically accessible for the singlet PES of $CH_2Cl + NO_2$ reaction. The CH_2Cl radical can barrierlessly react with NO_2 at the middle-N site to form the low-lying adduct **a** H_2ClCNO_2. Subsequently, isomer **a** most favorably isomerizes to $\mathbf{b_1}$ $H_2ClCONO$-*trans* that both **Path 1** and **Path 2** involve. Starting from $\mathbf{b_1}$, **Path 1** leading to product $\mathbf{P_1}$ $CH_2O + ClNO$ is more feasible than **Path 2** forming $\mathbf{P_2}$ CHClO + HNO because the transition states $\mathbf{TSb_1P_1}$(−34.1 kcal/mol) and $\mathbf{TSb_2P_1}$(−32.2 kcal/mol) in **Path 1** lie 12.0 and 10.1 kcal/mol lower than $\mathbf{TSb_1P_2}$(−22.1 kcal/mol) in **Path 2**, respectively. It should be noted that at low pressure, the ClNO molecule of $\mathbf{P_1}$ can be formed with an excess of vibrational energy, leading easily to its dissociation to Cl and NO. Therefore, except for the high-pressure regime, the system starting from the reactants **R** has enough energy to form $\mathbf{P_5}$ $CH_2O + Cl + NO$. As a result, reflected in the final product distribution, we predict that the primary $\mathbf{P_1}$ $CH_2O + ClNO$ is kinetically the most feasible product at high pressure, while at low pressure, the secondary product $\mathbf{P_5}$ $CH_2O + Cl + NO$ may have predominant yields; $\mathbf{P_2}$ CHClO + HNO may be the less competitive product.

To further testify the reaction mechanism obtained at the MC–QCISD//B3LYP level, we performed additional G2(B3LYP/MP2/CC) single-point energy calculations for the most relevant species based on the B3LYP/6–311*G*(d,p) geometries. As given in Table 1, the G2 (B3LYP/MP2/CC) and MC–QCISD single-point energies are generally in good agreement with each other. The largest deviation between the two levels is 3.7 kcal/mol for $\mathbf{TSb_1P_2}$. However, such a discrepancy will not affect our discussion on the reaction mechanism. It is easily found from Table 1 that the features of PES obtained at the G2(B3LYP/MP2/CC)//B3LYP level are in general consistent with those at the MC–QCISD//B3LYP level. (1) All the intermediates and transition states in Paths 1 and 2 lie below the reactants **R** at the two levels. So the two pathways are both thermodynamically and kinetically feasible at low temperature. (2) Most importantly, both the level-based calculations predict that Path 1 is more competitive than Path 2 because starting from the common isomer $\mathbf{b_1}$, the relative energies of $\mathbf{TSb_1P_1}$ and $\mathbf{TSb_2P_1}$ in Path 1 are lower than that of $\mathbf{TSb_1P_2}$ in Path 2. (3) The primary product $\mathbf{P_1}$ (CH_2O+ClNO) can further dissociate to the secondary product $\mathbf{P_5}$ (CH_2O+Cl+NO) at both levels. Because this paper mainly concerned with the reaction mechanism, we except that the present MC–QCISD//B3LYP results could be reliable for the title reaction.

Our result is in good agreement with kinetic study results by Timonen et al. [14] that the observed major product is CH_2O, which can be found as one species in the most favorable product $\mathbf{P_1}$ $CH_2O + ClNO$ in

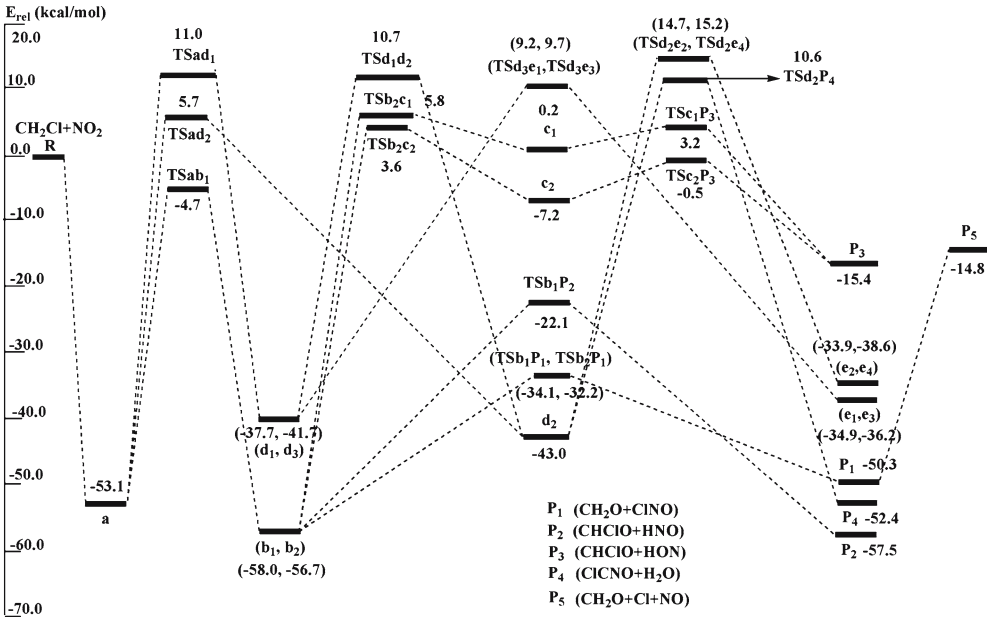

Fig. 2 Schematic singlet potential energy surface of the relevant reaction pathways for the $CH_2Cl + NO_2$ reaction. Relative energies (E_{rel}) (kcal/mol) are calculated at the MC–QCISD//B3LYP/6–311G(d,p) + ZPE level

our calculations. Formation of NO was also detected, but because of the production of radicals other than CH_2Cl in the photolysis or in the secondary chemistry and their possible reactions with NO_2 to produce NO, it was impossible to assign the origin of NO unambiguously to the $CH_2Cl + NO_2$ reaction in the experiment of Timonen et al. While, based on our present calculations, we make sure that the further dissociation of ClNO in primary **P$_1$** can produce species NO. Because all the involved intermediates and transition states in **Path 1** and **Path 2** lie below the reactants **R**, the $CH_2Cl + NO_2$ reaction is expected to be fast even at low temperatures. This is also consistent with the experimental measurement by Timonen et al. [14] in which the measured rate constant of this reaction at room temperature was 2.16×10^{-11} cm^3 molecule^{-1} s^{-1}, and the reaction of $CH_2Cl + NO_2$ is thus expected to contribute to the elimination of nitrogen dioxide pollutants and may be of significance in atmospheric chemistry. In fact, Timonen et al. stated

> In addition, several other potential products were searched. The absence of a measurable ion signal in these cases cannot be taken as a proof of the insignificance of these possible products in reaction $CH_2Cl + NO_2$ because the sensitivity of our experimental system is not known for these species.

Therefore, further kinetic investigations are still required for the unobserved low-lying products ClNO, CHClO, and HNO, and to deeply understand the mechanism of the title reaction.

4 Conclusions

The detailed mechanistic study on the radical–molecule reaction $CH_2Cl + NO_2$ has been reported at the B3LYP and MC–QCISD (single-point) levels. (1) This reaction proceeds most likely through the singlet CH_2ClNO_2 PES initiated by the carbon-to-nitrogen attack barrierlessly leading to adduct **a** H_2ClCNO_2 followed by isomerization to **b$_1$**$H_2ClCONO$-*trans*. (2) Starting from **b$_1$**, two primary products **P$_1$** CH_2O + ClNO and **P$_2$** CHClO + HNO, and one secondary product **P$_5$**CH_2O + Cl + NO should be observed, in which **P$_1$** is the most favorable product at high pressure, while at low pressure, **P$_5$** may be the most competitive. **P$_2$** is the less feasible product. Our results agree well with the experimental observation for the title reaction. (3) Since all the involved intermediates and transition states in the feasible pathways **Paths 1** and **2** are lower than the reactants **R** in the energy, the CH_2Cl+NO_2 reaction is expected to be fast, which is consistent with the experimental measurement, and thus the title reaction may play an important part in atmospheric chemistry, which are related to the prompt NO_x-formation and NO_x-reduction mechanism [20,21]. The present theoretical studies may provide useful information on the reaction mechanism and assist in further laboratory identification of the products for the title reaction.

Acknowledgments This work is supported by the National Natural Science Foundation of China (20333050, 20303007), the Doctor Foundation by the Ministry of Education, the Foundation for University Key Teacher by the Ministry of Education, the Key Subject of Science and Technology by the Ministry of Education of China, and the Key subject of Science and Technology by Jilin Province.

References

1. Baren RE, Erickson MA, Hershberger JF (2002) Int J Chem Kinet 34:12
2. Rim KT, Hershberger JF (1998) J Phys Chem A 102:4592
3. Lanier WS, Mulholland JA, Beard JT (1988) Symp (Int) Combust [Proc] 21:1171
4. Chen SL, McCarthy JM, Clark WD, Heap MP, Seeker WR, Pershing DW (1988) Symp (international) combust [Proc] 21:1159
5. Myerson AL (1975) In: 15th Symposium (international) on combustion. The combustion Institute, Pittsburgh, PA, p 1085
6. Song YH, Blair DW, Siminski VJ, Bartok W (1981) In: 18th Symposium (international) on combustion. The Combustion Institute, Pittsburgh, PA, p 53
7. Chen SL, McCarthy JM, Clark WD, Heap MP, Seeker WR, Pershing DW (1986) In: 21st Symposium (international) on combustion. The Combustion Institute, Pittsburgh, PA, p 1159
8. Tsang W (1990) Combust Sci Technol 74:99
9. Violi A, D'Anna A, D'Alessio A (2001) Chemosphere 42:463
10. Tsang W, Hampson RF (1986) J Phys Chem Ref Data 15:1087
11. Warnatz J (1984) In: Gardiner WC Jr (ed) Combustion Chemistry. Springer, New York
12. Knyazev VD, Slagle IR (1998) J Phys Chem A 102:1770
13. Faravelli T, Frassoldati A, Ranzi E (2003) Combust Flame 132:188
14. Eskola AJ, Geppert WD, Rissanen MP, Timonent RS, Halonen L (2005) J Phys Chem A 109:5376
15. Frisch MJ, Trucks GW, Schlegel HB, Scuseria GE, Robb MA, Cheeseman JR, Montgomery JA Jr, Vreven T, Kudin KN, Burant JC, Millam JM, Iyengar SS, Tomasi J, Barone V, Mennucci B, Cossi M, Scalmani G, Rega N, Petersson GA, Nakatsuji H, Hada M, Ehara M, Toyota K, Fukuda R, Hasegawa J, Ishida M, Nakajima T, Honda Y, Kitao O, Nakai H, Klene M, Li X, Knox JE, Hratchian HP, Cross JB, Adamo C, Jaramillo J, Gomperts R, Stratmann RE, Yazyev O, Austin AJ, Cammi R, Pomelli C, Ochterski JW, Ayala PY, Morokuma K, Voth GA, Salvador P, Dannenberg JJ, Zakrzewski VG, Dapprich S, Daniels AD, Strain MC, Farkas O, Malick DK, Rabuck AD, Raghavachari K, Foresman JB, Ortiz JV, Cui Q, Baboul AG, Clifford S, Cioslowski J, Stefanov BB, Liu G, Liashenko A, Piskorz P, Komaromi I, Martin RL, Fox DJ, Keith T, Al-Laham MA, Peng CY, Nanayakkara A, Challacombe M, Gill PMW, Johnson B, Chen W, Wong MW, Gonzalez C, Pople JA (2003) Gaussian 03, Revision B.04. Gaussian, Pittsburgh PA
16. Fast PL, Truhlar DG (2000) J Phys Chem A 104:6111 (2000)
17. Bauschlicher CW, Partridge H (1995) J Chem Phys 103:1788
18. Kuchitsu K (1998) Structure of free polyatomic molecules basic data; Springer-Verlag: Berlin, Germany
19. Lide DR (1999) In CRC handbook of chemistry and physics, 80th edn. CRC Press, Boca Raton
20. Miller JA, Bowman CT (1989) Prog Energy Combus Sci 15:287
21. Strobel DF (1982) Planet Space Sci 30:839